(2)

ARMY RESEARCH LABORATORY

Barium Strontium Titanate and Non-Ferroelectric Oxide Ceramic Composites for Use in Phased Array Antennas

L. C. Sengupta, S. Stowell, E. Ngo, M. O'Day,
and R. Lancto

ARL-TR-342 April 1994

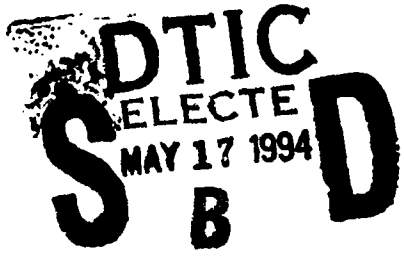

The findings in this report are not to be construed as an official Department of the Army position unless so designated by other authorized documents.

Citation of manufacturer's or trade names does not constitute an official endorsement or approval of the use thereof.

Destroy this report when it is no longer needed. Do not return it to the originator.

REPORT DOCUMENTATION PAGE

Form Approved
OMB No. 0704-0188

1. AGENCY USE ONLY (Leave blank)	2. REPORT DATE	3. REPORT TYPE AND DATES COVERED
	April 1994	Final Report

4. TITLE AND SUBTITLE
Barium Strontium Titanate and Non Ferroelectric Oxide Composites for Use in Phased Array Antennas

5. FUNDING NUMBERS

6. AUTHOR(S)
L. C. Sengupta, S. Stowell, E. Ngo, M. O'Day, and R. Lancto'

7. PERFORMING ORGANIZATION NAME(S) AND ADDRESS(ES)
U.S. Army Research Laboratory
Watertown, MA 02172-0001
ATTN: AMSRL-MA-CA

8. PERFORMING ORGANIZATION REPORT NUMBER
ARL-TR-342

9. SPONSORING/MONITORING AGENCY NAME(S) AND ADDRESS(ES)
U.S. Army Research Laboratory
2800 Powder Mill Road
Adelphi, MD 20783-1197

10. SPONSORING/MONITORING AGENCY REPORT NUMBER

11. SUPPLEMENTARY NOTES
Presented at the Intergrate Ferroelectrics, Monterey, CA March 14-16, 1994.

12a. DISTRIBUTION/AVAILABILITY STATEMENT
Approved for public release; distribution unlimited

12b. DISTRIBUTION CODE

13. ABSTRACT *(Maximum 200 words)*

A ceramic ferroelectric phase shifting device has been demonstrated using $Ba_{1-x}Sr_xTiO_3$ (BSTO) ceramics.[1] As part of an effort to optimize the electronic device performance in the phase shifter, various composites of BSTO combined with other nonelectrically active oxide ceramics have been formulated. In general the composites have reduced dielectric constants, ε', where $\varepsilon = \varepsilon' - i\varepsilon''$ and loss tangents, tan δ. The low dielectric constant and low loss tangent reduce the overall impedance mismatch and insertion loss of the device. In addition, the overall tunability, change in the dielectric constant with applied voltage, is maintained at a relatively high level (15% with an applied electric field of 1.5 V/μm) for dielectric constants of 200. The combination of electronic properties of these materials offer substantially higher operating frequencies, 10 GHz and above. The microstructures including grain size and phase analysis have been examined using SEM and EDX. X-ray diffraction has been used to identify compositions of any secondary phases formed in the composites. The analysis of the phase formation and compositional variations will be related to the electronic properties of the materials.

14. SUBJECT TERMS	15. NUMBER OF PAGES
Ferroelectric, phase shifter, ceramic composite, phased array antennas, barium strontium titanate	18
	16. PRICE CODE

17. SECURITY CLASSIFICATION OF REPORT	18. SECURITY CLASSIFICATION OF THIS PAGE	19. SECURITY CLASSIFICATION OF ABSTRACT	20. LIMITATION OF ABSTRACT
Unclassified	Unclassified	Unclassified	UL

Contents

Figures

Tables

1. INTRODUCTION

Phased array antennas can steer transmitted or received signals either linearly or in two dimensions without mechanically oscillating the antenna. These antennas are currently constructed using ferrite phase shifting elements. Due to the type of circuit requirements necessary to operate these antennas, they are costly, large and heavy. Therefore, the use of these antennas has been limited primarily to military applications which are strategically dependent on such capabilities. In order to make these devices available for many other commercial and military uses, the basic concept of the antenna must be improved. If ferroelectric materials could be used instead of ferrites, phased array antennas would be totally revolutionized.

A ceramic Barium Strontium Titanate, $Ba_{1-x}Sr_xTiO_3$, (BSTO), electro-optic phase shifter using a planar microstrip construction has been demonstrated.[1] In order to meet the required performance specifications, maximum phase shifting ability, the electronic properties in the low frequency (KHz) and microwave regions (GHz) must be optimized. As part of this optimization process, various composites of BSTO and non-ferroelectric oxides have been formulated. The BSTO-Alumina composite has a patent pending on its formulations and the other composites which are designated herein as BSTO-Oxide II and BSTO-Oxide III currently have a patent undergoing the filing process. All of these composites possess improved electronic properties. The comparison of the compositions and phase formation of the various BSTO-oxide ceramic composites will be made and related to their electronic properties. This report will outline some of the initial findings and compare them to the results found for pure BSTO.

2. EXPERIMENTAL

2.1 Ceramic Processing

Powder forms of Barium Titanate and Strontium Titanate were obtained from Ferro Corporation, Transelco Division, Pen Yan, N.Y. (product nos. 219-6 and 218 respectively), stoichiometrically mixed to achieve $Ba_{.6}Sr_{.4}TiO_3$ and ball-milled in ethanol using 3/16" alumina media for 24 hrs. The resulting BSTO was then air-dried, calcined at 1100^0C and mixed with either powder alumina (ALCOA Industrial Chemicals, Bauxite, AR, distributed by Whittaker, Clark, and Daniels, South Plainfield, N.J., product no. A16-SG) or a second oxide (oxide II) or a third oxide (oxide III) in the proper weight percent and ball-milled again in a slurry of ethanol using the alumina grinding media for an addtional 24 hrs.

3 wt% of Rholpex B-60A (Rohm and Haas Co., Philadephia, PA) binder is added to the resulting BSTO/oxide mixture. The mixture is then air-dried and dry-pressed uniaxially to a pressure of approximately 7000 p.s.i.. Sintering schedules were obtained by employing a deflectometer such as Mitutoyo digimatic indicator and miniprocessor (Mitutoyo Corp., Paramus N.J.). The densities, % Porosity and % Absorption are given in Table I. Results were obtained by performing an immersion density in ethanol using a modified ASTM standard. It should be noted that all of the examined samples have % liquid absorption of less than 2%.

Two metallization techniques were employed one involved painting on two circular, aligned electrodes, one on either side of the specimens, using high purity silver paint (SPI Supplies West Chester, PA) and attaching wires using high purity silver epoxy, Magnobond 8000, made by Magnolia Plastics, Inc., Chamblee, GA. The other technique utilized

the screen printing of electrodes using silver conductive ink (FERRO #3350, Electronic Materials Division, Santa Barbara, CA) and wires were attached by dipping the specimens in a bath of 2% silver, 62% tin and 36% lead solder.

2.2 Electronic Measurements

The dielectric constants, ε', loss tan δ, % tunability were determined for all composites. The dielectric constant, ε', where

$$\varepsilon = \varepsilon' - i\varepsilon'' \quad (1)$$

is a complex function. The loss tan δ can be defined as:

$$\tan \delta = \varepsilon'' / \varepsilon' \quad (2)$$

and the % tunability of a material is determined using the following equation:

$$\% \text{ tunability} = \{ \varepsilon'(0) - \varepsilon'(Vapp)\} / \{\varepsilon'(0)\} \quad (3)$$

The tunability measurements were taken with an applied electric field which ranged from 0 to 3.0 V/micron (μm). The electronic properties given in the tables were measured at a frequency of 1 KHz. Capacitance measurements for all materials were taken using an HP4284A LCR meter and the dielectric constants were calculated using equation (4) and the sample dimensions.

$\varepsilon' = Ct/A\varepsilon_0$ where (4)

ε' = dielectric constant of the layer
C = capacitance of BSTO
t = thickness
A = area
$\varepsilon_0 = 8.8542 \times 10^{-12}$ F/m

Further calculations were done to correct for the effect of fringe capacitance. The dielectric constant has been calculated from corrected capacitance values, C_{corr}, according to equation (5). The edge (fringe) capacitance, C_e, was calculated from either equation (6) or (7) depending on electroding configuration. These equations assume that the ground capacitance is zero and the thickness of the metal layer is much less than the thickness of the specimen.

$C_{corr} = C_{meas} - C_e$ where C_{meas} = measured capacitance value and C_e is defined below (5)

Equal electrodes smaller than the specimen:

$$C_e = (0.0019\, C_{meas} - 0.00252 \ln t + 0.0068)\, P \quad (6)$$

TABLE I Sample Descriptions of BSTO-Oxide Ceramic Composites.

BSTO-Alumina

Additive Content (wt%)	*Density (g/cc)*	*% Porosity*	*% Absorption*
0 wt% Al_2O_3	5.373	3.16	0.48
1 wt% Al_2O_3	5.319	8.94	1.43
5 wt% Al_2O_3	4.744	6.63	1.10
10 wt% Al_2O_3	4.687	7.15	1.22
20 wt% Al_2O_3	4.222	7.81	1.46
30 wt% Al_2O_3	3.965	5.05	1.03
60 wt% Al_2O_3	3.797	5.47	1.20
80 wt% Al_2O_3	3.615	7.48	1.72
pure Al_2O_3	3.992	4.44	0.95

BSTO-Oxide II

Additive Content (wt%)	*Density (g/cc)*	*% Porosity*	*% Absorption*
1 wt% Oxide II	5.22	10.31	1.64
5 wt% Oxide II	5.28	8.86	1.51
10 wt% Oxide II	5.30	7.67	1.23
15 wt% Oxide II	5.12	8.27	1.28
20 wt% Oxide II	5.37	10.31	1.64
25 wt% Oxide II	5.44	14.24	2.33
30 wt% Oxide II	5.40	9.73	1.60
40 wt% Oxide II	5.36	10.59	1.67
50 wt% Oxide II	5.22	10.34	1.70
60 wt% Oxide II	5.38	10.28	1.58

BSTO-Oxide III

Additive Content (wt%)	*Density (g/cc)*	*% Porosity*	*% Absorption*
1 wt% Oxide III	5.00	10.70	1.94
5 wt% Oxide III	5.30	3.97	0.63
10 wt% Oxide III	5.19	3.36	0.55
15 wt% Oxide III	4.95	5.38	0.97
20 wt% Oxide III	5.03	5.25	0.87
25 wt% Oxide III	4.81	3.30	0.55
30 wt% Oxide III	4.69	4.27	0.81
40 wt% Oxide III	4.42	5.40	0.98
50 wt% Oxide III	4.11	5.16	0.99
60 wt% Oxide III	3.94	2.56	0.75
80 wt% Oxide III	3.52	10.34	1.87

Diameter of the electrodes = diameter of the specimen.

$$C_e = (0.0041\ C_{meas} - 0.0034 \ln t + 0.0122)\ P \quad (7)$$

where $P = \pi (d_{electrode} + t)$ and $d_{electrode}$ = diameter of the electrode and t =thickness of the specimen.

3. RESULTS AND DISCUSSION

3.1 SEM and EDX Analysis

SEM examination of the individual bulk ceramic layers of the BSTO-Alumina composite revealed that a second phase became apparent in alumina additions as low as 10 wt% becoming more dominant at 35 wt% alumina and then disappearing by the time 60 wt% is achieved. Micrographs for these microstructures are displayed in Figs. 1(a) - 1(c). EDX of the small grains revealed a depletion in alumina while EDX of the larger, smoother grains displayed an increase in the alumina content. This suggests the formation of a barium aluminum titanium oxide phase.

SEM examination of the individual BSTO-Oxide II and BSTO-Oxide III compositions showed very little microstructural difference with added percentages of oxide. A small reduction in grain size was the most apparent difference. A micrograph of typical BSTO-Oxide II and BSTO-Oxide III microstructures are shown in Figs. 2(a) and (b) . EDX analysis of the individual layers showed no unusual behavior with the percentage of oxide II or oxide III gradually increasing with steady decreases in barium, strontium and titanium.

3.2 X-Ray Diffraction

A summary of the X-Ray diffraction results for the various compositions of the BSTO composites are given in Table II. It should be noted that there are three different forms of Barium Aluminum Oxide listed within the table. In agreement with EDX, the results reveal that when alumina is added to BSTO in small amounts, < 20 wt%, a second phase of Barium Aluminum Titanate, $Ba_3Al_{10}TiO_{20}$, is formed. In compositions having between 20 and 40 wt% alumina another second phase of Barium Aluminum Titanate forms ie. $BaAl_6TiO_{12}$. In this composition range we are also seeing traces of Barium Aluminum Oxide. By the time the composition reaches 60 wt% alumina no forms of Barium Aluminum Titanate are detectable. Only faint traces of BSTO are discernible at this composition. At 60 wt% alumina we were unable to discern which phase was most prevalent or even if all three phases were present. At 80 wt% alumina a specific phase of Barium Aluminum Oxide still could not be identified, but definite Al_2O_3 peaks became apparent. Pure alumina provided a complete diffraction pattern.

The results for the BSTO-Oxide II composites reveal a completely different picture. The results observed for these composites show that initially oxide II appears to be absorbed into the BSTO lattice structure. At compositions from 5-50 wt% oxide II, BSTO is the more dominant pattern, but at 60 wt%, oxide II becomes predominant. It is also interesting to note that no second phase materials were detected at any of the compositions for this composite. Similar results were observed for the BSTO-Oxide III composites. The only variation for this composite is that traces of oxide III are apparent even with only a 1 wt% additon.

TABLE II X-Ray Diffraction Results.

BSTO-Alumina

Oxide Content	*Detected Phases*
pure BSTO	Full pattern for $Ba_{.6}Sr_{.4}TiO_3$
1 wt% Al_2O_3	BSTO and $Ba_3Al_{10}TiO_{20}$
5 wt% Al_2O_3	BSTO and $Ba_3Al_{10}TiO_{20}$
10 wt% Al_2O_3	BSTO and $Ba_3Al_{10}TiO_{20}$
15 wt% Al_2O_3	BSTO and $Ba_3Al_{10}TiO_{20}$
20 wt% Al_2O_3	BSTO. $Ba_3Al_{10}TiO_{20}$ and $BaAl_{13.2}O_{20.8}$
25 wt% Al_2O_3	BSTO. $Ba_3Al_{10}TiO_{20}$. $BaAl_6TiO_{12}$ and $BaAl_{13.2}O_{20.8}$
30 wt% Al_2O_3	$Ba_3Al_{10}TiO_{20}$. $BaAl_6TiO_{12}$. BSTO and $BaAl_{13.2}O_{20.8}$
35 wt% Al_2O_3	$Ba_3Al_{10}TiO_{20}$. $BaAl_6TiO_{12}$. BSTO and $BaAl_{13.2}O_{20.8}$
40 wt% Al_2O_3	$Ba_3Al_{10}TiO_{20}$. $BaAl_6TiO_{12}$. BSTO and $BaAl_{13.2}O_{20.8}$
60 wt% Al_2O_3	Barium Aluminum Oxide - phase unknown and BSTO
80 wt% Al_2O_3	Barium Aluminum Oxide - phase unknown and Al_2O_3
pure Al_2O_3	Full Al_2O_3 pattern

3.3 Electronic Properties

The results for the electronic properties of the BSTO-Alumina composites are shown in Table III. The dielectric constant of the specimens is quickly reduced for compositions up to 35 wt% alumina at which point the rate of reduction in the dielectric constant is diminished. The dielectric loss, tan δ, reported here for all specimens includes the loss caused by the metal contact, improved metallization for these materials will definitely result in loss tan $\delta < 0.01$. The % tunability of the specimens could be increased with an increase in applied field and by using thinner specimens. Even so, the tunability of the composites is maintained at reasonable levels (>10%) up to 20 wt% alumina at which time the tunability decreases rapidly. A graph of the Tunability versus Applied Field is shown in Fig. 3. The inset shows the Dielectric Constant of these compositions versus Tunability at an electric field of 0.7 V/μm.

TABLE III Electronic Properties of BSTO (Ba = .6) and Alumina Ceramic Composites.

Alumina Content (wt %)	*Dielectric Constant*	*Loss Tangent*	*% Tunability*	*Electric Field (V/μm)*
0.0	3299.08	0.0195	19.91	0.73
1.0	2606.97	0.0122	22.50	0.76
5.0	1260.53	0.0630*	13.88	0.67
10.0	426.74	0.0163	4.79	0.39
15.0	269.25	0.0145	5.72	0.87
20.0	186.01	0.0181	3.58	0.48
25.0	83.07	0.0120		
30.0	53.43	0.0135	5.13	2.21
35.0	27.74	0.0029	0.51	0.83
40.0	25 62	0.1616*		
60.0	16.58	0.0009	0.01	0.60
80.0	12.70	0.0016		
100.0	8.37	0.0036		

* samples had poor contacts

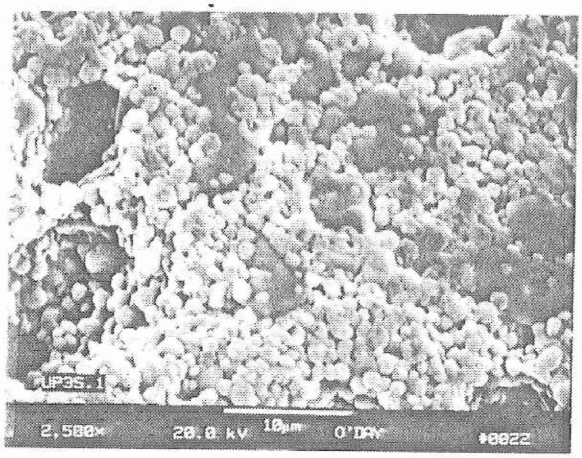

(a)

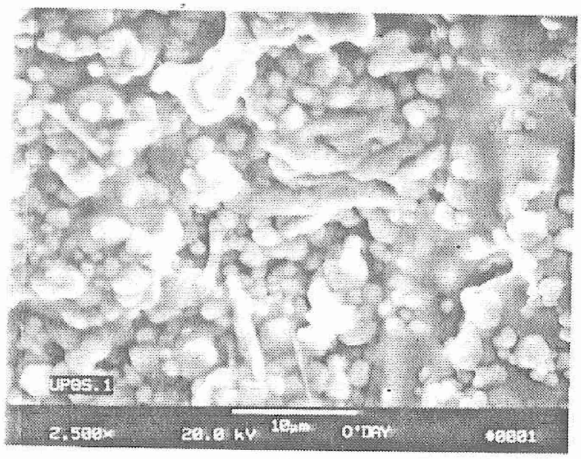

(b)

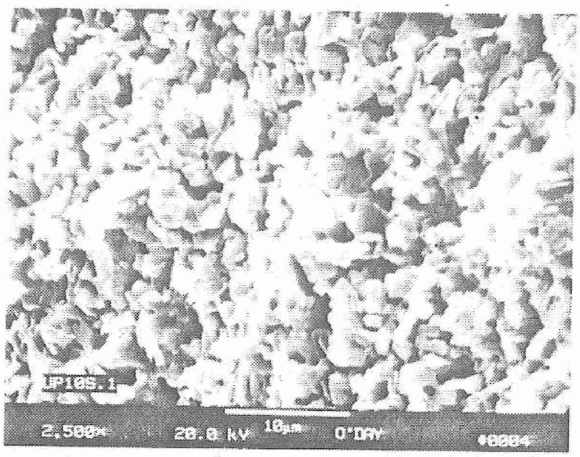

(c)

FIGURE 1 (a) SEM micrograph of BSTO-10 wt% Alumina bulk ceramic composite microstructure, (b) SEM micrograph of BSTO-35 wt% Alumina bulk ceramic composite microstructure, (c) SEM micrograph of BSTO-60 wt % Alumina bulk ceramic composite microstructure.

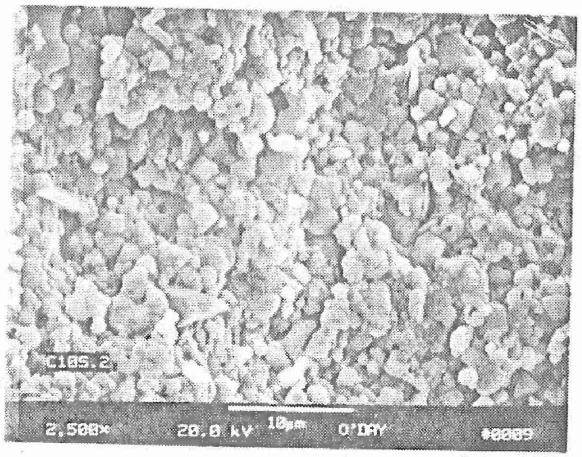

(a)

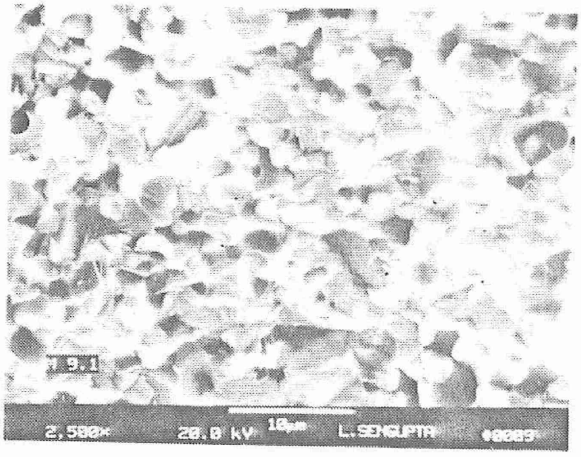

(b)

FIGURE 2 (a) SEM micrograph of BSTO-40 wt% Oxide II buik ceramic composite microstructure, (b) SEM micrograph of BSTO-40 wt% Oxide III bulk ceramic composite microstructure.

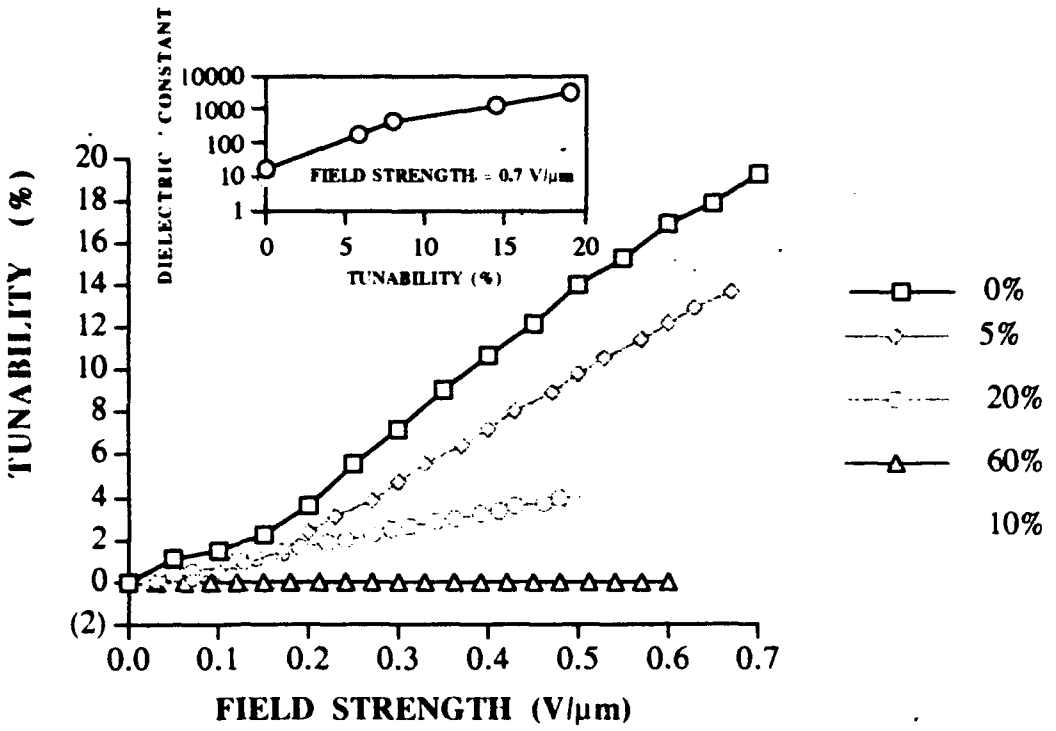

FIGURE 3 Tunability (%) versus Applied Electric Field (V/μm) for BSTO-Alumina composites (inset shows the Dielectric Constant versus Tunability (%) at an electric field of 0.7 V/μm).

Table IV contains the electronic data for the BSTO-Oxide II ceramic composites. As shown in Table IV the loss tangent of the materials are relatively low (<0.02). It appears that as the dielectric constant decreased the loss was lowered. The dielectric constant of the composites decreases with the addition of oxide II. The semi-log plot of the dielectric constants of the BSTO-Alumina composites, the BSTO-Oxide II composites and the BSTO-Oxide III composites is shown in Fig. 4. As shown in Fig. 4, the rate of reduction is similar for both composites for compositions < 20 wt%. However, between 20 wt% - 50 wt% the rate of reduction in the dielectric constant is less than that of the BSTO-Alumina composites. The decrease in the dielectric constant for the two sets of composites is again similar from 60 wt%-100 wt% additive content. However, the magnitude of the dielectric constant for all of the BSTO-Alumina composites is less than that of the BSTO-Oxide II and BSTO-Oxide III composites. This may be due to the formation of the second phases in the BSTO-Alumina composites.

The Tunability (%) versus Applied Electric Field for several compositions of BSTO-Oxide II composites is shown in Fig. 5. The inset represents the Dielectric Constant of these compositions versus Tunability (%) at an electric field of 0.7 V/μm. It is apparent that the tunability decreases for compositions less than 30 wt% oxide II. For additive contents >25 wt% and at similar electric fields, the tunability of the BSTO-Oxide II composites is greater than that of the BSTO-Alumina composites. This may again be due to the formation of second phases in the BSTO-Alumina composites, creating additional non-ferroelectric phases which inhibit tuning in the material.

TABLE IV Electronic Properties of BSTO-Oxide II Ceramic Composites.

Oxide II Content (wt %)	*Dielectric Constant*	*Loss Tangent*	*% Tunability*	*Electric Field (V/μm)*
0.0	3299.08	0.0195	19.91	0.73
1.0	2696.77	0.0042	46.01	2.72
5.0	2047.00	0.0138	12.70	0.76
10.0	1166.93	0.0111	7.68	0.68
15.0	413.05	0.0159	5.07	1.11
20.0	399.39	0.0152	5.39	0.76
25.0	273.96	0.0240	6.02	1.02
30.0	233.47	0.0098	1.21	0.73
35.0	183.33	0.0091	5.87	0.95
40.0	162.26	0.0095	0.70	0.71
50.0	92.73	0.0071	1.67	1.12
60.0	69.80	0.0098		
80.0	17.31	0.0056		
100.0	15.98	0.0018	0.05	0.27

TABLE V Electronic Properties of BSTO-Oxide III Ceramic Composites.

Oxide III Content (wt %)	*Dielectric Constant*	*Loss Tangent*	*% Tunability*	*Electric Field (V/μm)*
0.0	3299.08	0.0195	19.91	0.73
1.0	1276.21	0.0015	16.07	2.32
5.0	1770.42	0.0014		
10.0	1509.19	0.0018		
15.0	1146.79	0.0011	7.270	1.91
20.0	1079.21	0.0009	15.95	2.33
25.0	783.17	0.0007	17.46	2.45
30.0	750.93	0.0008	9.353	1.62
35.0	532.49	0.0006	18.00	2.07
40.0	416.40	0.0009	19.81	2.53
50.0	280.75	0.0117*	9.550	2.14
60.0	117.67	0.0006	11.08	2.70
80.0	17.00	0.0008	0.61	1.72
100.0	13.96	0.0009		

* samples had poor contacts

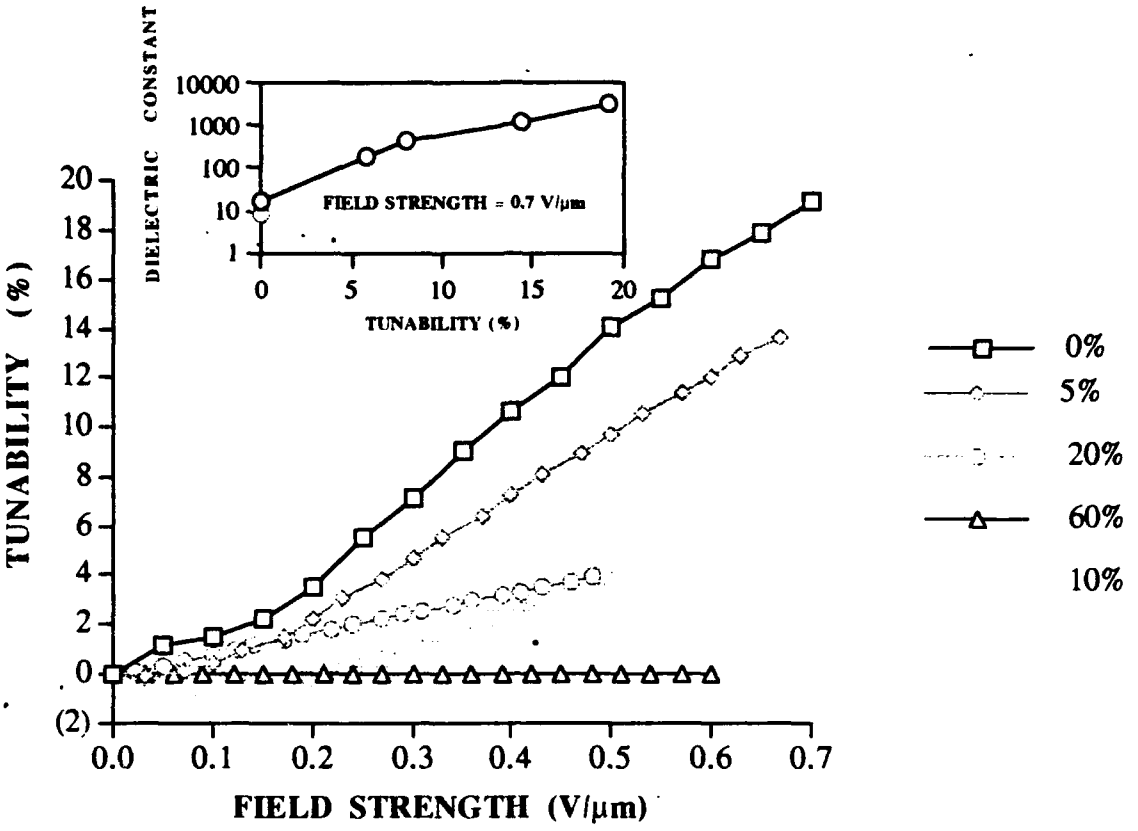

Fig. 4. Tunability (%) versus Applied Electric Field (V/μm) for BSTO-Oxide II composites (inset shows the Dielectric Constant versus Tunability (%) at an electric field of 0.7 V/μm).

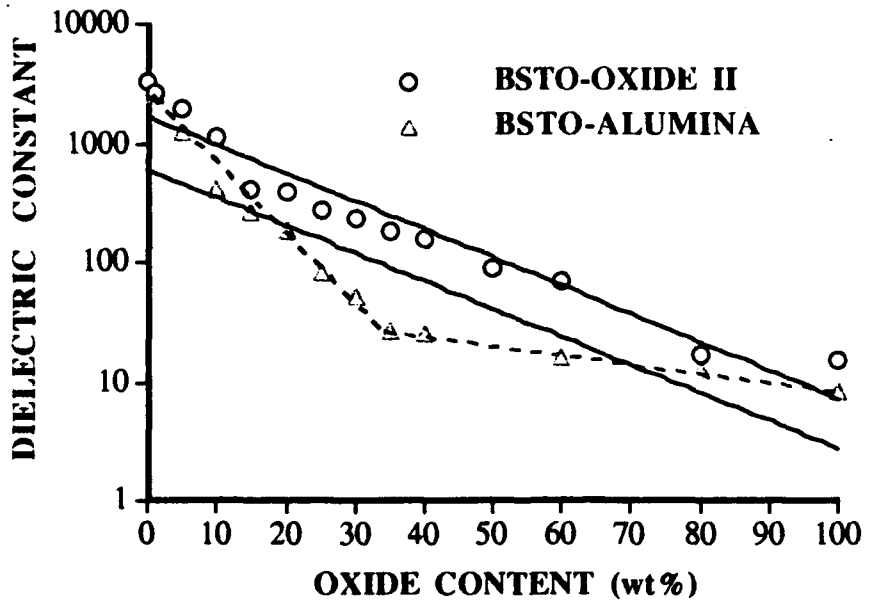

Fig. 5. Semi-log plot of the Dielectric Constant versus Alumina and Oxide II Content for BSTO-Alumina and BSTO-Oxide II composites.

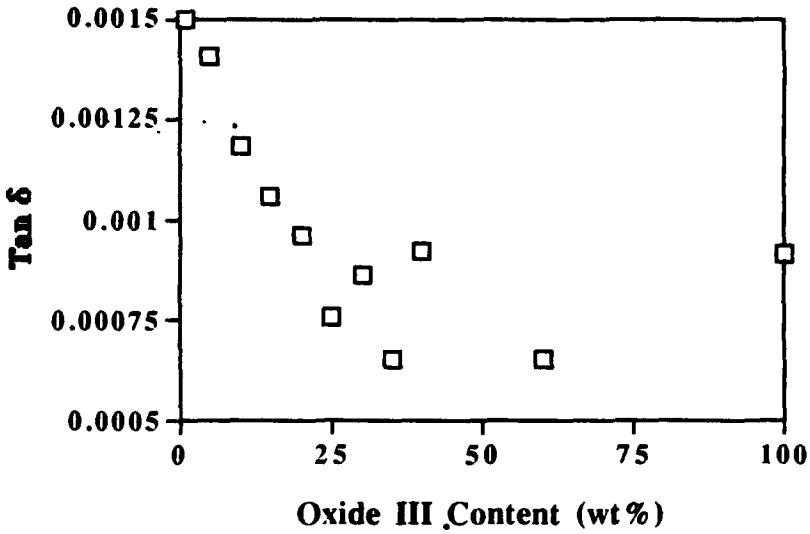

FIGURE 6 Loss Tangent versus Oxide III Content (wt %) for BSTO-Oxide III composites.

The electronic data for the BSTO-Oxide III composites is shown in Table V. As shown in Fig. 6, the loss tangent of the composites are extremely low for most all composition (decreases slightly with an increase in oxide III). These formulations could therefore be used at much higher operating frequencies, i.e., at millimeter wave range, @ 77 GHz. As shown in Fig. 4, the other electronic properties are similar to BSTO-Oxide II, except for the fact that the dielectric constants are even higher for these composites in the range 15-60 wt%. The tunability decreases slowly with increase in oxide III content and the composites exhibit high tunabilities (>10%) up to 60 wt% oxide III which was not the case for the other oxides.

4. CONCLUSIONS

Composites of BSTO and non-ferroelectric oxide ceramics have been fabricated and characterized. The composites have all demonstrated adjustable electronic properties. The dielectric constant of the BSTO-Alumina composites decreases faster than the BSTO-Oxide II and the BSTO-Oxide III composites from 20-50 wt% alumina content and is related to the formation of multiple second phases in this composition range for the BSTO-Alumina composites. The BSTO-Oxide III composites exhibited the lowest loss (<0.001) and highest dielectric constants in the composition range from 15-60 wt% oxide content. The low loss of the BSTO-Oxide III composites makes higher operating frequencies i.e, millimeter wave range, 77 GHz possible.

5. ACKNOWLEDGMENTS

The authors would like to thank Philip Wong, ARL-MD, for his contributions to the SEM and EDX work in this paper. Also, the assistance of Daniel Snoha and Kyu Cho, ARL-MD, with "all" of the X-ray diffraction data is greatly appreciated.

6. REFERENCES

1. R.W. Babbitt, T. E. Koscica, and W.E. Drach, "Planar Microwave Electro-optic Phase Shifters," *Microwave Journal*, **35** [6] 63-79 (1992).

DISTRIBUTION LIST

No. of Copies	To
1	Office of the Under Secretary of Defense for Research and Engineering, The Pentagon, Washington, DC 20301
	Director, U.S. Army Research Laboratory, 2800 Powder Mill Road, Adelphi, MD 20783-1197
1	ATTN: AMSRL-OP-SD-TP, Technical Publishing Branch
1	AMSRL-OP-SD-TM, Records Management Administrator
	Commander, Defense Technical Information Center, Cameron Station, Building 5, 5010 Duke Street, Alexandria, VA 23304-6145
2	ATTN: DTIC-FDAC
1	MIA/CINDAS, Purdue University, 2595 Yeager Road, West Lafayette, IN 47905
	Commander, Army Research Office, P.O. Box 12211, Research Triangle Park, NC 27709-2211
1	ATTN: Information Processing Office
	Commander, U.S. Army Materiel Command, 5001 Eisenhower Avenue, Alexandria, VA 22333
1	ATTN: AMCSCI
	Commander, U.S. Army Materiel Systems Analysis Activity, Aberdeen Proving Ground, MD 21005
1	ATTN: AMXSY-MP, H. Cohen
	Commander, U.S. Army Missile Command, Redstone Arsenal, AL 35809
1	ATTN: AMSMI-RD-CS-R/Doc
	Commander, U.S. Army Armament, Munitions and Chemical Command, Dover, NJ 07801
2	ATTN: Technical Library
	Commander, U.S. Army Natick Research, Development and Engineering Center, Natick, MA 01760-5010
1	ATTN: Technical Library
	Commander, U.S. Army Satellite Communications Agency, Fort Monmouth, NJ 07703
1	ATTN: Technical Document Center
	Commander, U.S. Army Tank-Automotive Command, Warren, MI 48397-5000
1	ATTN: AMSTA-ZSK
1	AMSTA-TSL, Technical Library
	Commander, White Sands Missile Range, NM 88002
1	ATTN: STEWS-WS-VT
	President, Airborne, Electronics and Special Warfare Board, Fort Bragg, NC 28307
1	ATTN: Library
	Director, U.S. Army Research Laboratory, Weapons Technology, Aberdeen Proving Ground, MD 21005-5066
1	ATTN: AMSRL-WT

No. of Copies	To
	Commander, Dugway Proving Ground, UT 84022
1	ATTN: Technical Library, Technical Information Division
	Commander, U.S. Army Research Laboratory, 2800 Powder Mill Road, Adelphi, MD 20783
1	ATTN: AMSRL-SS
	Director, Benet Weapons Laboratory, LCWSL, USA AMCCOM, Watervliet, NY 12189
1	ATTN: AMSMC-LCB-TL
1	AMSMC-LCB-R
1	AMSMC-LCB-RM
1	AMSMC-LCB-RP
	Commander, U.S. Army Foreign Science and Technology Center, 220 7th Street, N.E., Charlottesville, VA 22901-5396
3	ATTN: AIFRTC, Applied Technologies Branch, Gerald Schlesinger
	Commander, U.S. Army Aeromedical Research Unit, P.O. Box 577, Fort Rucker, AL 36360
1	ATTN: Technical Library
	U.S. Army Aviation Training Library, Fort Rucker, AL 36360
1	ATTN: Building 5906-5907
	Commander, U.S. Army Agency for Aviation Safety, Fort Rucker, AL 36362
1	ATTN: Technical Library
	Commander, Clarke Engineer School Library, 3202 Nebraska Ave., N, Fort Leonard Wood, MO 65473-5000
1	ATTN: Library
	Commander, U.S. Army Engineer Waterways Experiment Station, P.O. Box 631, Vicksburg, MS 39180
1	ATTN: Research Center Library
	Commandant, U.S. Army Quartermaster School, Fort Lee, VA 23801
1	ATTN: Quartermaster School Library
	Naval Research Laboratory, Washington, DC 20375
2	ATTN: Dr. G. R. Yoder - Code 6384
	Chief of Naval Research, Arlington, VA 22217
1	ATTN: Code 471
	Commander, U.S. Air Force Wright Research & Development Center, Wright-Patterson Air Force Base, OH 45433-6523
1	ATTN: WRDC/MLLP, M. Forney, Jr.
1	WRDC/MLBC, Mr. Stanley Schulman
	U.S. Department of Commerce, National Institute of Standards and Technology, Gaithersburg, MD 20899
1	ATTN: Stephen M. Hsu, Chief, Ceramics Division, Institute for Materials Science and Engineering

No. of Copies	To
1	Committee on Marine Structures, Marine Board, National Research Council, 2101 Constitution Avenue, N.W., Washington, DC 20418
1	Materials Sciences Corporation, Suite 250, 500 Office Center Drive, Fort Washington, PA 19034
1	Charles Stark Draper Laboratory, 555 Technology Square, Cambridge, MA 02139
	Wyman-Gordon Company, Worcester, MA 01601
1	ATTN: Technical Library
	General Dynamics, Convair Aerospace Division, P.O. Box 748, Fort Worth, TX 76101
1	ATTN: Mfg. Engineering Technical Library
	Plastics Technical Evaluation Center, PLASTEC, ARDEC, Bldg. 355N, Picatinny Arsenal, NJ 07806-5000
1	ATTN: Harry Pebly
1	Department of the Army, Aerostructures Directorate, MS-266, U.S. Army Aviation R&T Activity - AVSCOM, Langley Research Center, Hampton, VA 23665-5225
1	NASA - Langley Research Center, Hampton, VA 23665-5225
	U.S. Army Vehicle Propulsion Directorate, NASA Lewis Research Center, 2100 Brookpark Road, Cleveland, OH 44135-3191
1	ATTN: AMSRL-VP
	Director, Defense Intelligence Agency, Washington, DC 20340-6053
1	ATTN: ODT-5A (Mr. Frank Jaeger)
	U.S. Army Communications and Electronics Command, Fort Monmouth, NJ 07703
1	ATTN: Technical Library
	U.S. Army Research Laboratory, Electronic Power Sources Directorate, Fort Monmouth, NJ 07703
1	ATTN: AMSRL-EP-M, W. C. Drach
1	AMSRL-EP-M, T. E. Koscica
1	AMSRL-EP-M, R. W. Babbit
	Director, U.S. Army Research Laboratory, Watertown, MA 02172-0001
2	ATTN: AMSRL-OP-WT-IS, Technical Library
25	Authors